Am J Physiol Heart Circ Physiol 320: H52–H65, 2021.
First published December 16, 2020; doi:10.1152/ajpheart.00420.2020

american physiological society

AMERICAN JOURNAL OF PHYSIOLOGY
HEART AND CIRCULATORY PHYSIOLOGY

RESEARCH ARTICLE

Vascular Biology and Microcirculation

Diet alters age-related remodeling of aortic collagen in mice susceptible to atherosclerosis

Shana R. Watson,[1] Kara M. Cooper,[1] Piaomu Liu,[2] Nazli Gharraee,[1] Liya Du,[1] Savannah M. Han,[1] Edsel A. Peña,[3] Michael A. Sutton,[4] John F. Eberth,[1] and Susan M. Lessner[1]

[1]*Department of Cell Biology and Anatomy, University of South Carolina School of Medicine, Columbia, South Carolina;* [2]*Department of Mathematical Sciences, Bentley University, Waltham, Massachusetts;* [3]*Department of Statistics, University of South Carolina, Columbia, South Carolina; and* [4]*Department of Mechanical Engineering, University of South Carolina, Columbia, South Carolina*

Abstract

Vascular cells restructure extracellular matrix in response to aging or changes in mechanical loading. Here, we characterized collagen architecture during age-related aortic remodeling in atherosclerosis-prone mice. We hypothesized that changes in collagen fiber orientation reflect an altered balance between passive and active forces acting on the arterial wall. We examined two factors that can alter this balance, endothelial dysfunction and reduced smooth muscle cell (SMC) contractility. Collagen fiber organization was visualized by second-harmonic generation microscopy in aortic adventitia of apolipoprotein E (apoE) knockout (KO) mice at 6 wk and 6 mo of age on a chow diet and at 7.5 mo of age on a Western diet (WD), using image analysis to yield mean fiber orientation. Adventitial collagen fibers became significantly more longitudinally oriented with aging in apoE knockout mice on chow diet. Conversely, fibers became more circumferentially oriented with aging in mice on WD. Total collagen content increased significantly with age in mice fed WD. We compared expression of endothelial nitric oxide synthase and acetylcholine-mediated nitric oxide release but found no evidence of endothelial dysfunction in older mice. Time-averaged volumetric blood flow in all groups showed no significant changes. Wire myography of aortic rings revealed decreases in active stress generation with age that were significantly exacerbated in WD mice. We conclude that the aorta displays a distinct remodeling response to atherogenic stimuli, indicated by altered collagen organization. Collagen reorganization can occur in the absence of altered hemodynamics and may represent an adaptive response to reduced active stress generation by vascular SMCs.

NEW & NOTEWORTHY The following major observations were made in this study: *1*) aortic adventitial collagen fibers become more longitudinally oriented with aging in apolipoprotein E knockout mice fed a chow diet; *2*) conversely, adventitial collagen fibers become more circumferentially oriented with aging in apoE knockout mice fed a high-fat diet; *3*) adventitial collagen content increases significantly with age in mice on a high-fat diet; *4*) these alterations in collagen organization occur largely in the absence of hemodynamic changes; and *5*) circumferential reorientation of collagen is associated with decreased active force generation (contractility) in aged mice on a high-fat diet.

active force; collagen; aging; apolipoprotein E; fiber angle; high-fat diet; vascular remodeling

INTRODUCTION

Vascular cells restructure extracellular matrix in response to aging or changes in mechanical loading (1–5). We hypothesized that changes in collagen fiber orientation, an underexplored aspect of vascular remodeling, reflect an altered balance between passive and active forces acting on the arterial wall. Therefore, we examined two factors that may alter this balance, endothelial dysfunction and reduced smooth muscle cell (SMC) contractility, in the apolipoprotein E (apoE) knockout (KO) mouse model of atherosclerosis during age-related aortic remodeling.

Atherosclerosis is a chronic inflammatory disease of the arterial intima, constituting a significant source of morbidity and mortality in the United States. Increasing age and elevated low-density lipoprotein cholesterol are known to be independent risk factors for the development of atherosclerosis (6). Apolipoprotein E is an essential ligand for the uptake and

S. M. Lessner (susan.lessner@uscmed.sc.edu).
Submitted 4 June 2020 / Revised 14 October 2020 / Accepted 14 October 2020

clearance of atherogenic lipoproteins. Mice with a genetic deficiency in apoE develop elevated plasma cholesterol levels, which lead to rapid and severe atherosclerosis (7, 8). The pathophysiology in apoE KO mice is similar to that in humans in regard to vascular distribution of lesions, cellular components, and overall lipid content of the lesions (9). Thus, apoE KO mice are regarded as one of the best small animal models for studying the development of atherosclerosis (10–12).

Many investigators have examined collagen deposition in atherosclerotic plaques in the apoE KO mouse, as well as in clinical specimens, based on the paradigm that collagen content of the fibrous cap is a key determinant of plaque stability or resistance to rupture (13–17), an important clinical target. In addition, compensatory outward remodeling of atherosclerotic vessels to maintain lumen cross section in the presence of plaque growth is a well-documented phenomenon (18–20). Akyildiz et al. (21) used diffusion tensor imaging to demonstrate complex collagen fiber architectures in human carotid atherosclerotic plaques, with multiple fiber orientations at different radial positions within the vessel wall. However, there has been much less attention paid to alterations in collagen architecture during vascular remodeling of the atherosclerosis-susceptible vessel before lesion formation. Agianniotis and Stergiopulos (22) reported that thoracic aortas of apoE KO mice on chow diet at 10–12 wk of age had significantly lower collagen content than those of matched wild-type C57BL/6 mice (7% vs. 20% area fraction, respectively). At the same time, the thoracic aortas of the apoE KO mice were stiffer than those of the controls, leading the authors to suggest that collagen fibers were recruited earlier under pressure loading in the apoE KO mice than in their wild-type counterparts (22). Cilla et al. (23) evaluated the in situ pressure-diameter behavior of descending thoracic and abdominal aorta in both C57BL/6 wild-type controls and apoE KO mice on chow diet, together with apoE KO mice on Western diet, as a function of age from 17 to 47 wk. Compared to 17-wk-old mice, older apoE KO mice on Western diet showed a progressive decrease in circumferential stretch ratio versus pressure that was absent in both groups of mice on the chow diet, together with significantly increased aortic stiffness after 30 wk of Western diet feeding (23). However, these authors did not evaluate changes in adventitial collagen deposition as a potential morphological correlate of increased circumferential stiffness.

A major pathological change often preceding the development of atherosclerosis and associated with vascular aging is endothelial dysfunction. Endothelial dysfunction denotes diminished production/availability of nitric oxide and/or an imbalance between vasoconstricting and vasodilating substances produced by or acting on the endothelium (24,25). The critical role of endothelial nitric oxide production in flow-induced vascular remodeling is now well established (26). However, a role for nitric oxide in maintaining mechanical homeostasis during vascular aging in the absence of altered hemodynamics remains to be confirmed. We reasoned that collagen fiber realignment may be influenced by endothelial dysfunction because nitric oxide production is essential to the maintenance of physiological contractile tone by arterial smooth muscle, and long-term changes in active contractile tone may be associated with compensatory alterations in passive mechanical behavior of the vessel (27). Therefore, we investigated both changes in active force generation by vascular SMCs and endothelial dysfunction as potential drivers of vascular remodeling and collagen fiber reorganization in the apolipoprotein E (apoE) knockout (KO) mouse.

In a previous study, we reported the use of a second harmonic generation (SHG) imaging technique to quantify collagen fiber distribution and alignment in the apoE KO mouse in lesion-free regions of the vessel wall. We employed a novel statistical analysis to study three dimensional (3D) fiber distribution and to provide details on differences in collagen fiber orientation in mice on a chow diet versus a Western diet (28). In this article, we have used an approach similar to that of Watson et al.(28) to report that diet alters age-related remodeling in the apoE knockout mouse model of atherosclerosis.

MATERIALS AND METHODS

Animals and Experimental Groups

For analysis of collagen content and organization, three sets of five apoE KO mice (9) (*Mus musculus*, B6.129P2-*Apoe*^{tm1Unc}/J, JAX stock no. 002052, Jackson Laboratory, Bar Harbor, ME; RRID:IMSR_JAX:002052) each were assigned to different treatment groups. Animals were assigned to groups consecutively on the basis of availability of litters. All groups received standard chow diet (Teklad Rodent Diet 8904, irradiated, Envigo, Indianapolis, IN) for the first 6 wk after weaning. The first group (two females, three males) was euthanized after 6 wk, whereas *group 2* (five males) was maintained on a chow diet for an additional 4.5 mo before euthanasia, and *group 3* (three males, two females) was transferred to a high-fat Western diet (4.5 kcal/g, 15 kcal% protein, 43 kcal% carbohydrates, and 42 kcal% fat) (stock no. TD.88137, Envigo, Indianapolis, IN) for an additional 6 mo and euthanized at 7.5 mo of age. The Western diet was used to promote hypercholesterolemia and atherosclerotic lesion formation within the aorta of the mice in *group 3*. Blood pressure measurements and ultrasonography were performed on all groups during the week preceding tissue harvest.

As described below, separate groups of apoE KO mice were used for wire myography experiments and for measurement of NO release by DAF-2 fluorescence, since these studies required fresh, unfixed tissue specimens. For the DAF-2 experiments, each group contained five mice. In both the chow diet groups, there were three males and two females. In the Western diet group, there were two males and three females. The entire thoracic aorta of each mouse was analyzed for the NO release experiments, as described below. For the myography experiments, each group contained seven mice. Both the 6-wk chow and 6-mo chow groups contained four males and three females, while the 6-mo Western diet group consisted of seven males. A single tissue ring from the descending thoracic aorta (region of the third to fourth intercostal arteries) was analyzed by wire myography.

All mice were handled in compliance with protocols approved by the University of South Carolina Institutional Animal Care and Use Committee.

In Vivo Physiological Measurements

Tail-cuff plethysmography.

Prior to blood pressure measurements, all mouse body weights (in grams) were recorded. Mouse blood pressure was

monitored by a tail-cuff blood pressure analysis system (MC4000; Hatteras Instruments, Cary, NC). Systolic and diastolic blood pressures were recorded over 5 preliminary equilibration cycles and 10 measurement cycles in awake mice. Mice were acclimated to the plethysmography system for 3 days minimum before the final blood pressure recording.

Ultrasonography.

Mice were anesthetized with 1.5–2.5% isoflurane in oxygen before and throughout ultrasound measurements on a Vevo 770 small animal ultrasound machine (Fujifilm VisualSonics, Toronto, ON, Canada). To acquire flow velocity and aortic inner diameter measurements in the thoracic aorta, mice were placed in a laterally recumbent position. For measurements in the abdominal aorta, mice were placed in a supine position. Ultrasound measurements correspond with the anatomical locations of collagen fiber measurements at the level of the fourth intercostal space and the abdominal aorta. B-mode images, pulsed-Doppler velocity measurements, and M-mode images were obtained using the RMV-707 probe (VisualSonics) with a broadband frequency up to 45 MHz. M-mode images were used to measure vessel diameter during systole and diastole. Volumetric flow rates were calculated from the mean aortic diameter and the time-averaged velocity, assuming Poiseuille flow behavior.

Sample Preparation

Following the duration of each diet, mice were ethically euthanized at 6 wk, 6 mo, or 7.5 mo of age by controlled-rate carbon dioxide asphyxiation. Following thoracotomy, mice were perfused through the left ventricle with heparinized normal saline (10 U/ml) for 5 min at physiological pressure, followed by pressure perfusion fixation for 10 min with 10% neutral buffered formalin. Thoracic and abdominal aortas were harvested from apoE KO mice from each age group and diet. One segment each from the thoracic and abdominal aortas was reserved for histology. For SHG microscopy analysis, nonlesioned areas of the aorta were sampled, with one segment taken at the level of the fourth intercostal arteries and one taken from the infrarenal abdominal aorta. Under a dissecting microscope, each aortic segment was opened longitudinally for en face examination. The specimens were flattened to a slide and labeled according to the direction of blood flow.

Second-Harmonic Generation Microscopy

To image collagen fibers, we used a custom-built hybrid two-photon excitation fluorescence (TPEF) second harmonic generation (SHG) microscope (29). Optical sectioning with SHG microscopy permits visualization of collagen fibers throughout the vessel wall thickness without staining. The SHG signals were collected from the forward direction through an Olympus 1.4 NA oil immersion condenser (29, 30). The XYZ stage of the microscope was controlled through three orthogonally mounted motors to collect image stacks throughout the vessel wall thickness using a ×60 objective. The area in pixels for each image was 512 × 512 pixels with the actual calibrated image being 176×176 μm. A few aortic specimens were counterstained with Hoechst 33258 nuclear stain (1:10,000 dilution) before imaging to confirm the flow direction, as indicated by alignment of endothelial cell nuclei, and the radial position of collagen fibers relative to the luminal surface.

Semiautomated Image Analysis

Using Continuity 6.4 b software, a previously described analytic protocol for automatic angle recognition (28, 31) was employed to quantify collagen fiber orientation. The software determined collagen fiber orientation using the circumferential (0°) and axial directions (±90°) as the reference points. The individual, local fiber orientations were determined in the z-θ plane. Each image of the stack was analyzed and provided fiber angle measurements to be used in a multivariate statistical analysis.

Linear Mixed-Effects Model

For this study, we constructed a linear mixed-effects model with random intercepts. The model is implemented using R package "lme4". The correlation of angle measurements on the same mouse is modeled by three random effects (i.e., random intercepts) in the model, which are the mouse random effect, the random effect of location [anatomic location (thoracic versus abdominal)] nested in mouse, and the random effect of depth (radial position) nested in location. The three random effects are independent normal random variables, each of which has mean 0 and positive variance. We denote the variances of the three random effects as σ^2_m, $\sigma^2_{l:m}$, and $\sigma^2_{c:l:m}$, respectively. To compare the mean absolute angle of the three groups of mice, we create a categorical variable ("group") with three levels to describe the age/diet information, where group = 0 labels the 6-wk mice fed with chow diet, group = 1 labels the 6-mo mice fed with chow diet, and group = 2 labels 6-mo mice fed with Western diet. To account for radial position within the artery wall, we investigated depth (radial position) as a categorical variable. An observation from depth in the first third of the image stack ($0 < t < 1/3$, where t is the wall thickness) relates to collagen fibers at the medial-adventitial boundary, an observation from the middle third ($1/3 < t < 2/3$) corresponds roughly to collagen fibers in the central adventitia, and an observation from the final third ($2/3 < t < 1$) is equivalent to fibers in the outer adventitia. We then create a three-level categorical variable ("catdep") to describe the depth information. If catdep = 0, a measurement is taken from the first third of the stack. If catdep = 1, a measurement is taken from the middle third of the stack. Measurements taken from the final third are given the value of catdep = 2. Fixed effects in the model are mouse group, anatomic location (thoracic versus abdominal), and radial position (catdep). The mean absolute angle can be calculated from the formula: E (Absolute Angle) = $\beta_0 + \beta_1$ (group 1) + β_2 (group 2) + β_3(location) + β_4(catdep1) + β_5 (catdep2), where E (Absolute Angle) is the mean absolute fiber angle for a given set of conditions, β_0 is the fixed intercept, and β_i are coefficients describing the contribution of each fixed effect. Fixed effects with $P < 0.05$ in the model were considered to be statistically significant contributors to the mean average absolute fiber angle.

Tissue Preparation for Histology

Fixed specimens from the third or fourth intercostal space and the infrarenal segment of mouse aortas were dehydrated

in graded alcohols and processed using conventional methods before paraffin embedding. Following embedding, the aortic segments were sectioned transversely at 5 μm to produce ring-shaped cross sections. In some cases, aortic samples were first embedded in 10% agarose gel for ease of handling and to obtain appropriate vertical orientation of the small specimens. In this process, cylindrical aortic segments were positioned horizontally in warm 10% agarose gel. After the gel had set, it was cut into blocks with the long axis of the block parallel to the vessel axis, dehydrated in graded alcohols, and processed using conventional methods for paraffin embedding. The blocks were oriented vertically during paraffin embedding to ensure that the aorta was sectioned transversely.

Collagen Content by Picrosirius Red Staining

Cross sections of aortic tissues were deparaffinized and rehydrated in descending grades of alcohol before incubation with Direct Red [0.1% in saturated picric acid; Sigma Aldrich, St. Louis, MA) for 90 min. The slides were washed in 0.01 N HCl and then dehydrated in ascending grades of alcohol and xylene before mounting with Permount. Picrosirius red (PSR)-stained tissue sections were analyzed by cross-polarized transmitted light microscopy on a Zeiss Axioskop 2 (Carl Zeiss Microscopy, Thornwood, NY). PSR-stained sections were imaged in bright-field for total area measurements and under cross-polarized transmitted light for collagen area measurement. Cross-polarized transmitted light images were segmented in ImagePro Plus software (Media Cybernetics, Silver Springs, MD) to measure the area of collagen birefringence in each aortic section. Fractional area of collagen was calculated as area of collagen birefringence (pixels)/total area of aortic wall (pixels) × 100%. A single section from each thoracic aorta was imaged for collagen analysis by PSR staining.

Collagen Type I Immunohistochemistry

For immunohistochemical detection of Type I collagen, we followed a standard protocol involving deparaffinization of the tissue, antigen retrieval with 10 mM citrate buffer, blocking with 10% donkey serum, staining with primary antibody against collagen type I (1:20 dilution, anticollagen type I rabbit polyclonal; MilliporeSigma, Burlington, MA; cat. no. 234167-500UL, RRID:AB_10682946), and visualization with a fluorescently labeled secondary antibody (1:50 dilution, Rhodamine Red X donkey anti-rabbit IgG, Jackson ImmunoResearch, West Grove, PA; RRID: AB_2340613). Negative controls consisted of sections processed in the absence of primary antibody. Nuclei were counterstained with Hoechst 33258 (1:10,000 dilution; Sigma Aldrich, St. Louis, MO). The epifluorescence microscope (Zeiss Axioskop 2) was equipped with a standard filter set to detect FITC (excitation 450–490 nm; emission 500–550 nm) and Rhodamine (excitation 538–562nm; emission 570–640nm). A charge-coupled device camera (Axiocam, Zeiss) with appropriate acquisition software (Axiovision, Zeiss) captured 8-bit images using the ×5 objective. The merged green (FITC channel) and red (Rhodamine channel) images provided the total vessel wall area, while the Rhodamine image provided the collagen area. Control sections were not stained with primary antibody and provided the baseline threshold to eliminate nonspecific background fluorescence. Images of control and experimental tissue samples were acquired at the same time using the same instrument settings. Epifluorescent images were segmented in ImagePro Plus software to measure the area of collagen I-specific staining in each aortic section. Fractional area of collagen I was calculated as area of collagen I staining (pixels)/total area of aortic wall (pixels) × 100%. A single section from each thoracic aorta was analyzed for collagen I content using this approach.

Nitric Oxide Synthase 3 Immunohistochemistry

Nitric oxide synthase 3 (NOS3) expression was evaluated by staining fixed cross sections of aortic specimens with a rabbit polyclonal antibody (pAb) to NOS3 (1:75 dilution) (Thermo Fisher Scientific cat. no. PA1-037, RRID: AB_325774). After deparaffinizing sections and blocking endogenous peroxidases with 3% hydrogen peroxide, antigen retrieval was performed using the citrate buffer technique. Sections were incubated with the primary antibody for 2 h. A biotinylated goat anti-rabbit secondary antibody (1:100 dilution; Jackson ImmunoResearch, RRID: AB_2337965) was used to detect the primary antibody and was visualized using horseradish peroxidase-conjugated streptavidin (1:250 dilution; Jackson ImmunoResearch, RRID: AB_2337238). Diaminobenzidine (DAB; Vector Laboratories) was used as the chromogen with a color development time set at 1.5 min. Negative controls consisted of sections stained in the absence of primary antibody. Sections were dehydrated in ascending grades of alcohol and Histoclear before mounting with Permount. Bright-field images were acquired on a Zeiss Axioskop and analyzed in ImagePro Plus by segmenting for DAB-stained area (brown color). Images of control and experimental tissue samples were acquired at the same time using the same instrument settings. Fractional area of NOS3 expression was calculated as area of DAB staining in the intima/total intimal area. Two individual sections were analyzed from each aortic ring and the results were averaged to represent each anatomic location from each animal.

Direct Measurement of NO with DAF-2

Acetylcholine-induced nitric oxide release was used as a second marker of endothelial dysfunction in a separate group of aortic specimens, using a modification of the method of Ozaki et al. (32). Mice (n = 5 per group, both sexes) were euthanized by carbon dioxide asphyxiation and perfused with heparinized saline (10 U/ml) through the left ventricle for 5 min. The entire thoracic aortic was excised, opened longitudinally, and mounted en face in a prepared pinning dish with stainless-steel insect pins. Specimens were refrigerated at 4°C in PBS (pH 7.4) for no more than 1 h before NO measurement, at which time the medium was replaced with 0.1 M phosphate buffer containing 1.5 mM calcium chloride. The samples were imaged before addition of 4,5-diaminofluorescein diacetate (DAF-2 DA) (negative control) with excitation at 465 nm and emission at 520 nm in an IVIS Spectrum imaging system (PerkinElmer, Waltham, MA). The IVIS settings used were field of view B, aperture F1, and small binning. Following baseline imaging, 50 μl of DAF-2 DA (Cayman Chemical, Ann Arbor, MI) was added to yield a final concentration of 10 μmol/l. After

a 5-min incubation, the sample was reimaged with the same settings. After 5-min incubation in the presence of 1 μM acetylcholine, the sample was again imaged at the same settings. NO release was measured as integrated fluorescence intensity over the tissue area in each image. The negative control value was used as a baseline and subtracted from the integrated intensity in the DAF-2 DA and ACh-treated samples.

Wire Myography for Active Force Measurement

Active and passive mechanical response to uniaxial loading was measured using a wire myograph (Radnoti, Covina, CA) for apoE KO mice at ages 6 wk and 6 mo on a chow diet and 6 mo on a Western diet. Seven mice per group (both sexes) were euthanized at each time point, and the descending thoracic aorta at the fourth intercostal region was harvested. All biomechanical measurements were done within 4 h after tissue harvest. Each aortic segment was mounted on two 50-μm wires and incubated for 30 min in oxygenated Krebs buffer at 37°C to equilibrate. The segments were then preconditioned by stretching three times to the normal stretch at physiological conditions. To measure the total force (F_T = active and passive), the aortic rings were treated with 10 μM phenylephrine in Krebs buffer to cause maximal contraction of SMCs. The initial distance (length) between two wires for the nonstretched state of the aorta was considered L_0. The segments were then stretched 100 μm at a time and kept for 3 min until the force stabilized. Images were taken at each stretch point to measure width (W) of the segment and the actual stretch which is denoted as L. The maximum circumferential stretch ratio varied from 1.8 to 2.3 for the 6-wk specimens and from 1.6 to 2.03 for the stiffer 6-mo specimens. These values were chosen to avoid breaking the aortic rings. To measure passive force (F_P), the aorta was brought back to L_0 and treated with 10 μM sodium nitroprusside (SNP) in Krebs buffer to cause complete relaxation of the SMCs and to inhibit active force generation. The rings were then stretched uniaxially in steps of 100 μm as described for total force measurement. Collected data were then processed to calculate active force (F_A) from the measured forces ($F_A = F_T - F_P$). To analyze the data, stretch ratio was measured from images as $\lambda = L/L_0$. Unloaded aortic thickness (t) was measured from ring images taken after myography, and segment width was measured from images to calculate stress as $s = \frac{F(mN)\cdot\lambda}{2\cdot w\cdot t(mm^2)}$. Relative active force was calculated at $(F_A/F_T)\times 100\%$ at the stretch value corresponding to the maximum active force value.

Statistical Analysis

For analysis of collagen content, maximum active stress generation, and active stress as a fraction of total stress, statistical differences among treatment groups were analyzed by one-way ANOVA followed by Tukey's test for multiple comparisons. For analysis of volumetric blood flow rate, NOS3 expression, and DAF-2 fluorescence, differences among treatment groups were analyzed by two-way ANOVA followed by Tukey's test for multiple comparisons. P values less than 0.05 were considered significant. Error bars in histograms (Fig. 10*C*) represent standard deviations.

RESULTS

Physiological Measurements

Body weight for 6-wk-old mice was found to be 16.4 ± 2.6 g. Mice consuming a Western diet for 6 mo demonstrated significantly increased body weight compared to 6-mo-old mice consuming a chow diet (31.0 ± 4.2 g vs. 24.5 ± 3.0 g, $P < 0.05$). However, despite the increase in body weight, systolic and diastolic aortic diameters measured using ultrasound were not significantly different between mice on a chow diet for 6 mo versus those on Western diet (Fig. 1). Similarly, aortic diameters did not increase significantly with age between 6 wk and 6–7.5 mo, despite a significant increase in body weight (Fig. 1).

As shown in Fig. 2, apoE KO mice on a Western diet for 6 mo had significantly lower systolic blood pressures by tail cuff plethysmography than 6-wk-old mice. However, there were no significant differences in diastolic blood pressures ($P > 0.05$ by ANOVA) or in calculated blood flow rates between the different treatment groups (Fig. 3).

Constructed three-dimensional histograms of collagen fiber distribution across aortic adventitia.

Figure 4 provides an illustration of representative three-dimensional (3D) histograms of adventitial collagen fiber angle distribution for apoE KO mice on chow diet at 6 wk old and 6 mo old and on Western diet at 7.5 mo old. Each 3D histogram reflects image stacks for one individual mouse on each diet with 0 degrees representing fibers oriented in the circumferential direction. The distribution of collagen fiber angles in the abdominal aortas is similar to that of the thoracic aortas but somewhat more disperse (Fig. 5).

Statistical analysis of collagen fiber distributions.

We report the estimates of model parameters, standard errors, and P values of the fixed effects in the linear mixed model (see Linear Mixed-Effects Model) in Table 1. In Table 2, we also report the same set of outputs from R of the final model. The final model is fit without the fixed effect (location), and we regroup the categorical variable (catdep) to

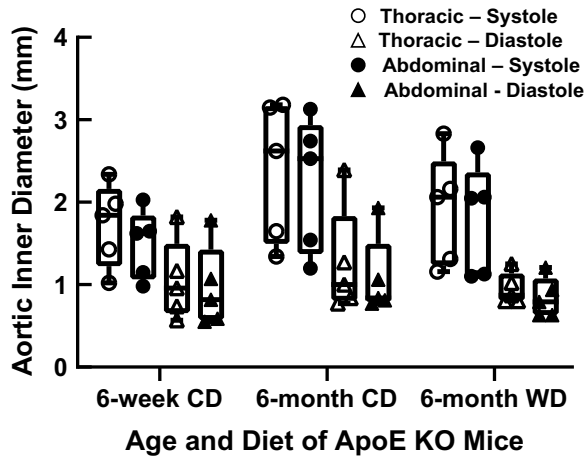

Figure 1. Systolic and diastolic aortic inner diameters obtained from ultrasound imaging for the three treatment groups ($n = 5$ per group). Two-way ANOVA showed that there was a significant effect of anatomic position (thoracic>abdominal; $P < 0.001$) for both systolic and diastolic diameters, but no significant differences among age/diet groups.

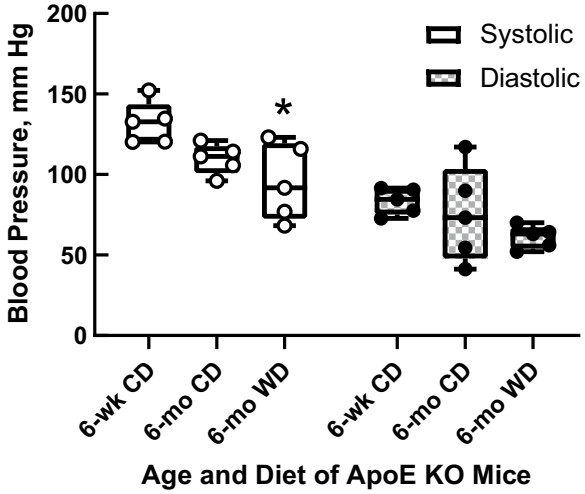

Figure 2. Systolic and diastolic blood pressure measurements from apolipoprotein E knockout (apoE KO) mice for the three treatment groups ($n = 5$ per group). Systolic blood pressure in mice on Western diet for 6 mo was significantly lower than 6-wk-old mice, but there were no significant differences in diastolic blood pressures between groups (one-way ANOVA followed by Tukey multiple-comparisons test). *$P < 0.05$ vs. 6 wk.

have just two levels because there is no difference in mean fiber angle between measurements taken from the first- and second-thirds of the stack. At $\alpha = 0.05$ level of significance, the anatomic location fixed effect is not statistically significant. After taking into account whether a measurement is taken from the last third of the stack, we conclude that the 6-mo mice fed with chow diet have mean fiber angle ~28° larger than that of the 6-wk mouse group, and the 6-mo mice fed the Western diet have mean fiber angle ~23° smaller than that of the 6-wk mouse group. We display the variance components estimates of the final model in Table 3.

Figure 6 shows a boxplot comparing the median, first, and third quartiles of collagen fiber angle observations for the

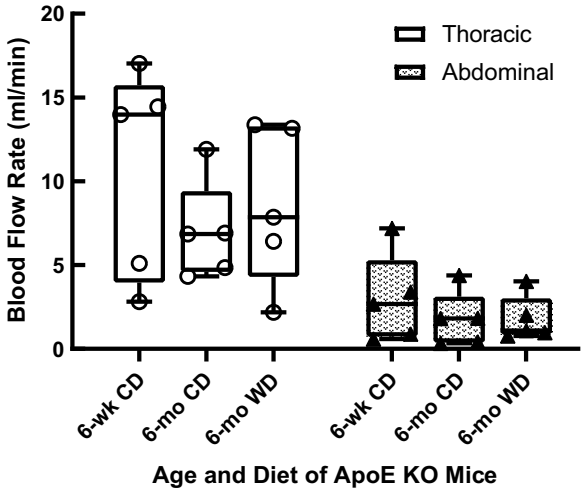

Figure 3. Mean volumetric blood flow rate acquired from Doppler ultrasonography of thoracic and abdominal aorta at 6 wk or after 6 mo on diet for the three treatment groups ($n = 5$ per group). No significant differences among treatment groups were detected by ANOVA.

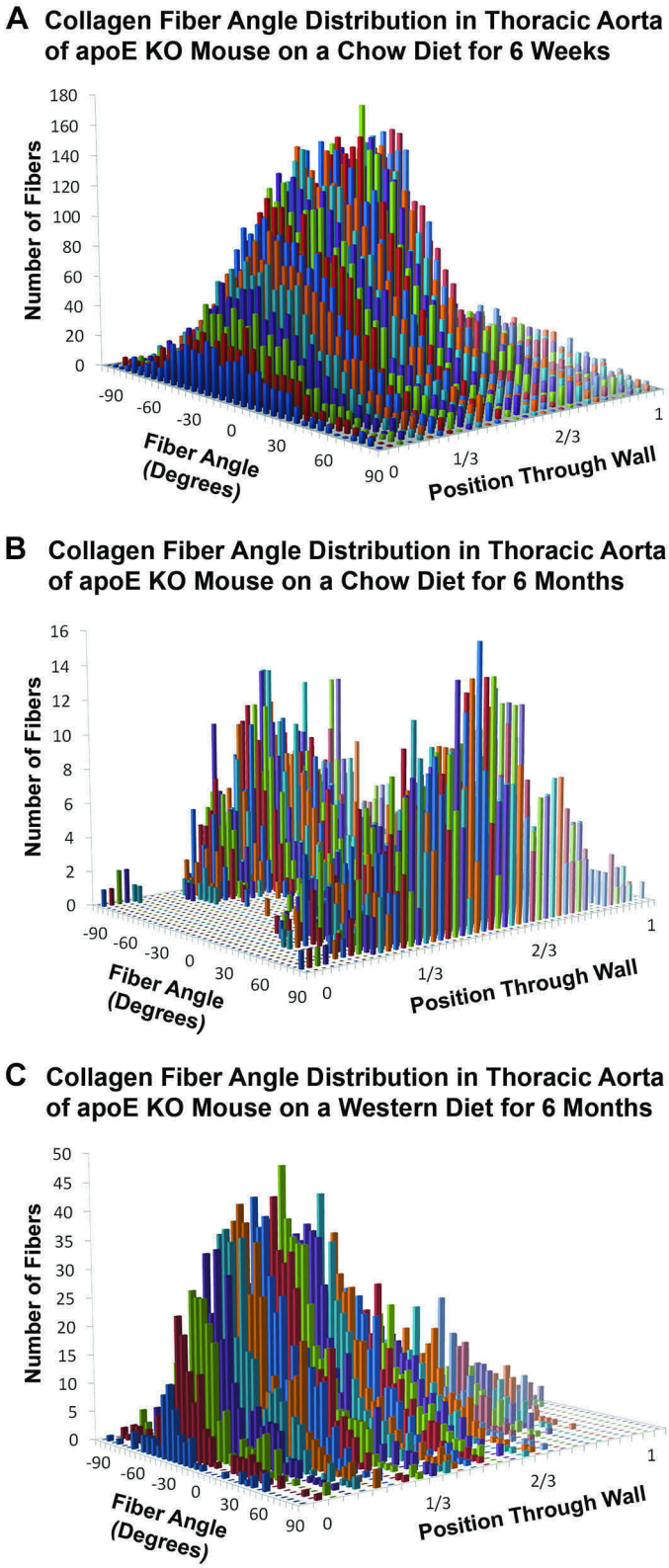

Figure 4. Representative three-dimensional histograms showing the distribution of collagen fiber angles in the adventitia of apolipoprotein E knockout (apoE KO) mice fed a chow diet for 6 wk (6 wk old; *A*), apoE KO mice fed a chow diet for 6 mo (~6 mo old; *B*), apoE KO mice fed a Western diet for 6 mo (~7.5 mo old; *C*). Circumferentially oriented fibers are given as 0° and axial fibers ±90°. The radial wall position is designated as zero at the medial-adventitial boundary and as one at the outer edge of the adventitia.

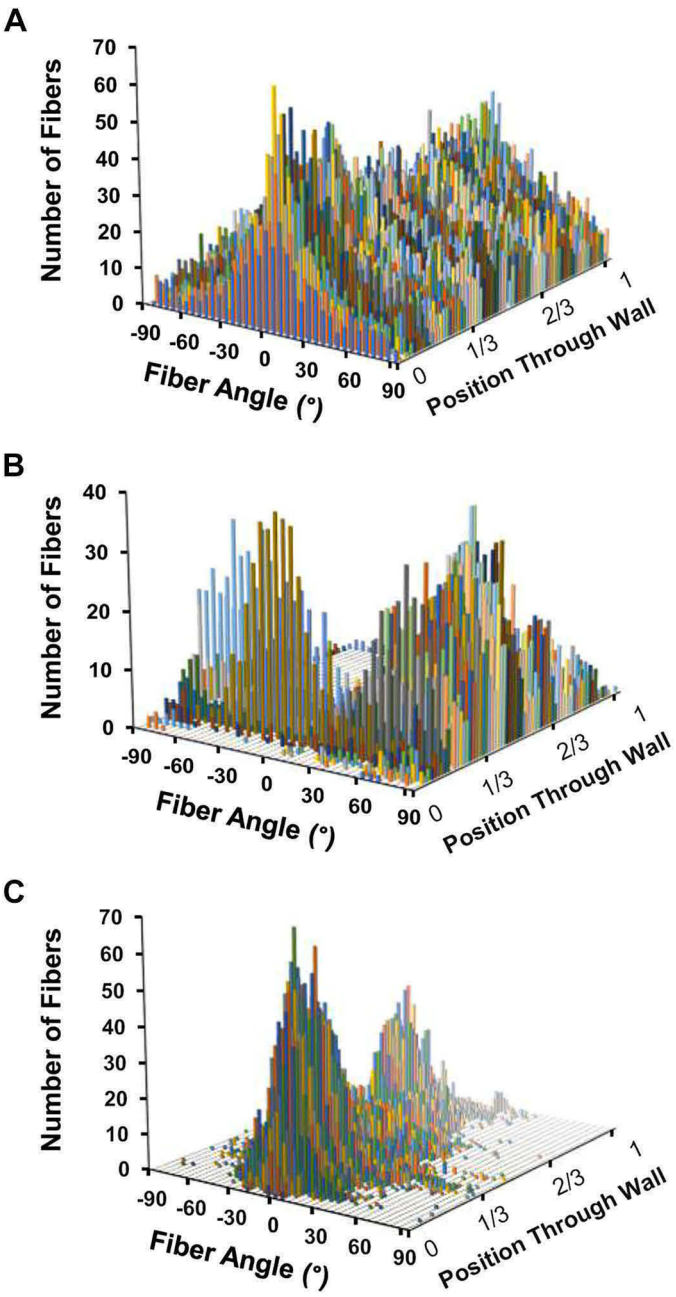

Figure 5. Representative three-dimensional histograms showing the distribution of collagen fiber angles in the infrarenal abdominal aorta of apolipoprotein E knockout (apoE KO) mice fed a chow diet for 6 wk (6 wk old; *A*), apoE KO mice fed a chow diet for 6 mo (~6 mo old; *B*), apoE KO mice fed a Western diet for 6 mo (~7.5 mo old; *C*). Circumferentially oriented fibers are given as 0° and axial fibers ± 90°. The radial wall position is designated as zero at the medial-adventitial boundary and as one at the outer edge of the adventitia.

apoE KO mice at different ages on a chow diet and on a Western diet after 6 mo.

Histological Analyses

Fractional collagen content (% area) for each of the three treatment groups obtained by Picrosirius red staining (Fig. 7) showed that collagen content increases significantly with age from 6 wk to 7.5 mo ($P < 0.05$). Qualitatively similar results were obtained from the collagen type I immunohistochemistry (IHC) analysis (Fig. 8). As age increased, aortic collagen type I content increased significantly; however, there were no statistical differences between older mice on different diets. The fractional collagen content measured by IHC was greater than that measured by PSR because PSR only shows mature, well-organized collagen that gives rise to birefringence. IHC shows all collagen type I, even immature or disorganized collagen.

NOS3 expression detected by immunoperoxidase staining was confined to the endothelial lining of the intima and to vasculature in the periadventitial fat (Fig. 9). In this study, we detected no significant differences in NOS3 expression by immunohistochemistry between any groups (Fig. 9, *bottom*).

Measurement of Nitric Oxide via DAF-2 in ApoE Knockout Mice

Figure 10 provides a bar and whisker graph illustrating the average nitric oxide (NO) expression for each experimental group, measured as integrated fluorescence intensity over the tissue area before and after addition of acetylcholine. While fluorescent intensity was significantly greater after addition of acetylcholine, there were no significant differences among treatment groups by two-way ANOVA.

Measurement of Active Force Generation by Aortic Rings

We used wire myography to study the effects of age and diet on contractility in the descending thoracic aorta of apoE KO mice after 6-wk chow, 6-mo chow, and 6-mo Western diet (Fig. 11). Young mice (6 wk) on chow diet show significantly higher maximum active stress generation compared to old mice (6 mo) on either chow or Western diet (102.0 ± 32.7 vs. 54.5 ± 19.3 and 23.2 ± 7.4 kPa, respectively). Moreover, older mice on Western diet have significantly lower active stress generation than those maintained on a chow diet.

DISCUSSION

Changes in collagen fiber arrangement represent a subtle form of vascular remodeling. Collagen fibers have preferred directions associated with the mechanical stresses on the tissue (33). Understanding the microscopic structure of collagen fibers and changes in their arrangement can provide information on how arteries remodel to maintain mechanical homeostasis. Quantitative analysis of collagen fiber angles from the atherosclerotic specimens used in our studies has been informative in defining the distribution of collagen and the factors that contribute to the remodeling capabilities of the aorta.

Our research has shown that, as apoE KO mice age, aortic adventitial collagen fibers redistribute to become more longitudinally oriented, increasing the average fiber angle by 27.8° (Table 2). The combination of a Western diet and aging resulted in a different rearrangement of collagen fibers, leading to an overall decrease in average fiber angle by 22.8°. With regard to the mean fiber angle, the structure-based constitutive model used by Collins et al. (34) predicted an angle of 39° with respect to the Z-direction (that is, 51° relative to

Table 1. *Parameter estimates of the linear mixed-effects model for 6-mo Western diet vs. 6-mo chow diet vs. 6-wk chow diet-fed apoE KO mice*

Variable	Coefficient	Estimate, Degrees	Standard Error	*P* Value
Intercept	β_0	35.05	1.896	<0.05
Six-month chow diet	β_1	27.75	2.399	<0.05
Six-month Western diet	β_2	−23.01	2.398	<0.05
Thoracic aorta	β_3	2.27	1.342	0.113
Central adventitial layer ($1/3 < t < 2/3$)	β_4	0.076	0.914	0.934
Outer adventitial layer ($2/3 < t < 1$)	β_5	2.14	0.913	0.023

Anatomic location (thoracic vs. abdominal) and radial position in the central adventitial layer (depth $1/3 < t < 2/3$) as fixed effects are not significant at the 0.05 level of significance in this model

the θ-direction) for normal (wild type) mouse infrarenal abdominal aorta. Similarly, Ferruzzi et al. (35) used biaxial mechanical test data to predict the average fiber angle values in the descending thoracic aorta and infrarenal aorta of B6 wild-type mice at 20 wk of age, obtaining values of 63.5° and 60.6°, respectively. Our observed mean fiber angle in the aortic adventitia is ∼36° in 6-wk-old chow diet-fed mice, somewhat lower than the predicted value. However, our result represents the experimental average of a three-dimensional distribution of fibers, as opposed to a parameter identified by fitting a four-fiber family model to biaxial test results. In addition, Collins et al. (34) studied mice that were 2–3 mo old, while Ferruzzi et al. used 5-mo-old mice (35). Consistent with their data, we observed a larger mean fiber angle (63.9°) in older apoE KO mice on the chow diet.

We found that there are no significant differences between the average absolute angles on the basis of anatomical location (thoracic vs. abdominal) in aging mice on either the chow diet or the Western diet (Table 1). Our data suggest that diet and age were the most significant factors causing alteration of the mean collagen fiber angle.

In trying to understand the cause of shifts in collagen fiber arrangement, we have assessed physiological factors, such as blood pressure (BP) and volumetric blood flow rate, which have previously been found to play an important role in driving geometrical arterial remodeling (36, 37). Our blood pressure results showed a significant reduction in systolic BP by 37 mmHg in apoE KO mice on a Western diet for 6 mo relative to 6-wk-old mice, but there were no significant differences in systolic BP between aged mice on chow diet versus those on Western diet and no significant differences in diastolic BP between any treatment groups. These results fall roughly within the range of BPs measured in several studies evaluating BP in young adult (12–34 wk of age) apoE KO mice fed either a standard chow diet or a Western-type diet (38–42). In contrast, Yang et al. (43) reported elevated BP in older (7.5 mo) apoE KO mice compared to 6-wk-old mice. It should be noted that a decrease in blood pressure would be expected to increase average collagen fiber angle relative to the circumferential direction, based strictly on passive mechanical response (44, 45), in contrast to our observation of decreased collagen fiber angle in the aged mice on a Western diet. Thus, it is unlikely that altered hemodynamics are mainly responsible for the reorganization of collagen in the Western diet-fed mice. Our blood flow rate measurements were similar to those acquired in vivo in the abdominal aorta of apoE KO mice using phase-contrast magnetic resonance imaging. Amirbekian et al. (46) recorded a mean blood flow rate in the apoE KO mouse infrarenal abdominal area of 2.95 ± 1.62 mL/min and a mean aortic diameter for the same area of 0.69 ± 0.04 mm. Our 6-wk-old mice had a mean blood flow rate of 2.95 ± 2.65 mL/min; however, we measured a larger abdominal aortic diameter at 0.96 ± 0.5 mm. These young mice did not show an aortic diameter or mean blood flow rate significantly different than older mice of the same strain on chow or Western diet.

Beyond hemodynamics, we also investigated total collagen content and looked for evidence of endothelial dysfunction by measuring NOS3 expression and acetylcholine-stimulated NO release (Fig. 10). Our data reveal that mature, birefringent collagen content, as well as collagen type I, increase significantly with aging in apoE KO mice on a Western diet. Although there was some apparent increase in adventitial collagen in older mice on a chow diet, it did not reach the level of statistical significance.

Previous studies detailing how endothelial dysfunction in the apoE KO mouse is influenced by aging, sex, and diet revealed that impaired endothelial nitric oxide-dependent relaxation response to acetylcholine, associated with plaque formation (47, 48), is aggravated by a Western-type diet (49, 50) and by aging (51, 52). We did not detect any significant differences in NOS3 protein expression by immunoperoxidase staining between older mice on either diet versus 6-wk-old mice, but the total endothelial area examined in aortic cross sections is very limited. To overcome this sampling limitation and to look for functional differences in NO production, we measured acetylcholine-induced NO release by

Table 2. *Parameter estimates of the final model without fixed location (thoracic aorta) and radial position in the central adventitial layer effects*

Variable	Coefficient	Estimate, Degrees	Standard Error	*P* Value
Intercept	β_0	36.10	1.610	<0.05
Six-month chow diet	β_1	27.78	2.220	<0.05
Six-month Western Diet	β_2	−22.79	2.223	<0.05
Outer adventitial layer ($2/3 < t < 1$)	β_3	2.14	0.742	0.007

Table 3. *Estimated variance components of the final linear mixed model*

	σ^2_m	$\sigma^2_{l:m}$	$\sigma^2_{c:l:m}$	Error Variance
Estimate	5.071	10.422	7.478	12.55

DAF-2 DA fluorescence in en face specimens of thoracic aorta. We found no significant differences between groups by ANOVA when considering both age and diet. This finding is contrary to published studies suggesting that nitric oxide release would decrease with age and atherogenic stimuli (48, 49). It should be noted that many of these previous studies used a different methodology, in which endothelial dysfunction is measured in aortic rings as reduced relaxation in response to acetylcholine. It is likely that the DAF-2 DA protocol for measuring NO production from intact aortic specimens lacks sufficient sensitivity to detect small differences between groups in our study. In the previous work by Ozaki et al. (32), the authors were able to detect a 1.5-fold increase in NO production in apoE/NOS3-Tg mice relative to apoE KO mice, but they also measured a 3.6-fold increase in aortic NOS3 protein by Western blot analysis in the apoE/NOS3 transgenics. They reported no detectable change in NO production between 12-wk old apoE KO mice and wild-type C57BL/6 mice.

To further investigate the cause of collagen fiber remodeling, circumferential uniaxial stretch tests were performed by wire myography on aortic rings taken from mice of corresponding ages and diets. Our data showed that there was a significant decrease in phenylephrine-induced active force generation with age, as well as a significant decrease in active forces in the older mice on a Western-style diet compared to those on chow diet. These data extend and complement previous work by Agianniotis and Stergiopulos (22) showing that apoE-deficient mice at 10–12 wk of age on a nonatherosclerotic diet have lower SMC contractility compared to their wild-type (WT) littermates. Using a biaxial inflation-extension test, these authors demonstrated that thoracic aortas of apoE-deficient mice showed lower maximum active diameters than WT under induced contractility.

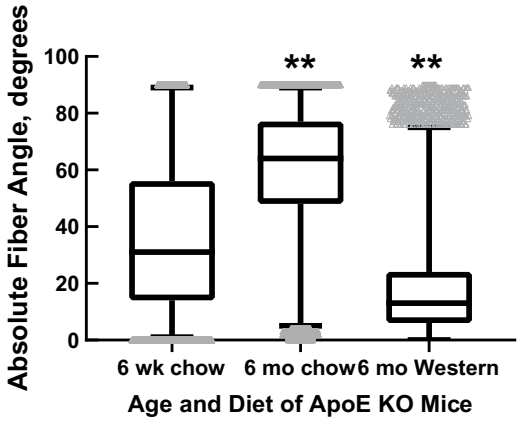

Figure 6. Average adventitial collagen fiber angle diverges with aging in apolipoprotein E knockout (apoE KO) mice on chow diet vs. those on Western diet ($n = 5$ mice per group). Compared to six-wk-old apoE KO mice, multivariate analysis showed a significant difference in average absolute fiber angle in response to age and a high-fat diet. On average, absolute fiber angle was increased by 27.8° in older mice on a chow diet and reduced by 22.8° in mice fed a Western diet for 6 mo. Whiskers show range 1–99%, with outliers in gray. $^{**}P < 0.001$.

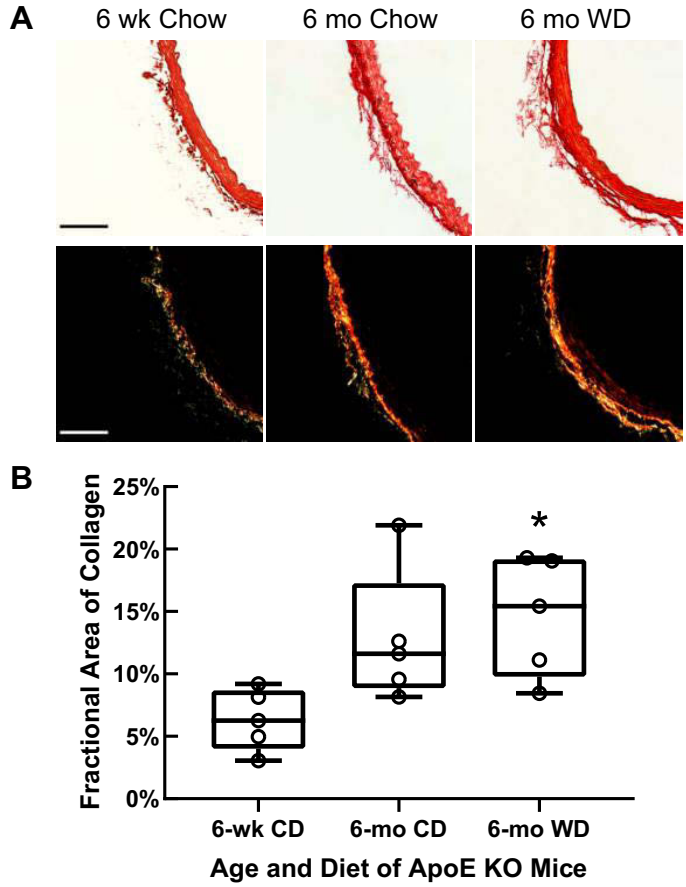

Figure 7. *A*: representative histological images of cross sections of descending thoracic aorta from 6 wk, 6-mo chow diet, and 6-mo Western diet apolipoprotein E knockout (apoE KO) mice. Brightfield images (×20) (top row) were used to obtain total area of vascular sections, while cross-polarized transmitted light images (×20) (bottom row) were employed to visualize the collagen content. *B*: fractional collagen content (% area) obtained by Picrosirius red staining for each of the three treatment groups ($n = 5$ per group). Collagen content increases with age, but differences become significant only in mice on a Western diet ($^*P < 0.05$ vs. 6 wk, ANOVA followed by Tukey multiple comparisons test). Scale bars = 100 μm. CD, chow diet; WD, Western diet.

We believe the reduction in active stress generation in older apoE KO mice could be due to a loss of SMC contractile phenotype, frequently reported in atherosclerosis (53). The loss of contractility can be attributed to either overt loss of contractile cells or to impaired activity of these cells. It is well established that smooth muscle cells are not terminally differentiated cells and can dedifferentiate to a synthetic phenotype if needed, based on environmental cues. Phenotypic switching (54) and apoptosis (55) of SMCs are known to happen at the site of atherosclerotic lesions. The same phenomena occurring in regions adjacent to lesions could explain our findings of lower contractility, since the synthetic phenotype does not show contractile properties. Moreover, SMCs are shielded by their local ECM from stresses applied to the vessel (56). As we demonstrate here, both collagen content and adventitial fiber orientation are affected by

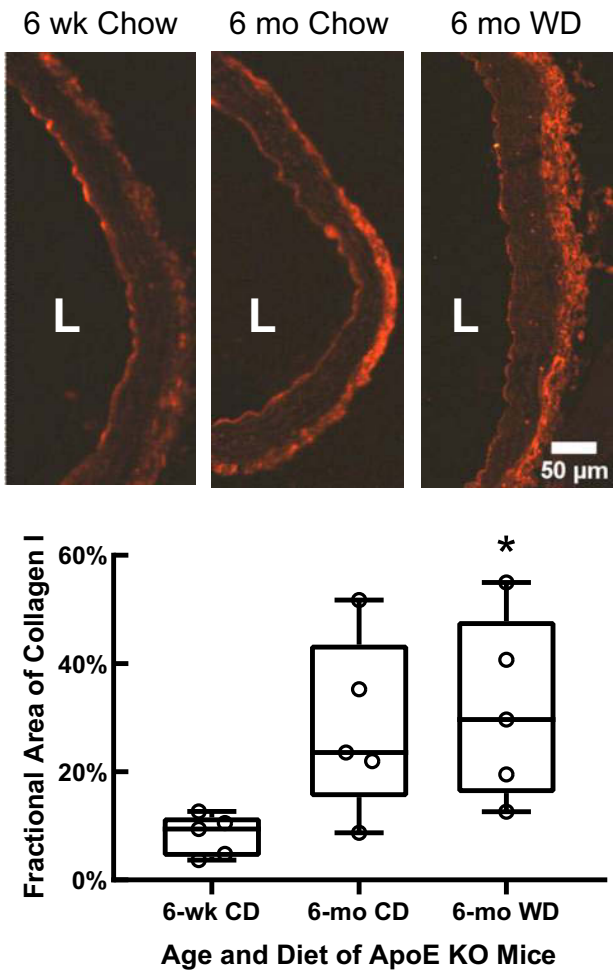

Figure 8. Collagen type I (% area) for each of the three treatment groups obtained from immunohistochemistry ($n = 5$ per group). *Top*: representative immunohistochemistry (IHC) images (red channel only) of aortic sections from each mouse group stained for collagen I, ×10 objective, scale bar = 50 μm. *Bottom*: collagen type I increases with age, but differences become significant only in mice on Western diet (*$P < 0.05$ vs. 6 wk, ANOVA followed by Tukey multiple comparisons test). The % collagen is greater by IHC, as opposed to PSR, because PSR only shows mature, well-organized collagen with birefringence. IHC shows all collagen type I, even immature. CD, chow diet; L, lumen; WD, Western diet. Scale bars = 50 μm.

age and diet. Stiffer, fibrotic matrix and reorientation of collagen fibers may alter local stress sensing by SMCs and, consequently, reduce contractility. Likewise, the capacity for the SMCs to generate active stresses and transmit those into overall vasoactive behavior depends on their interaction with the fibrous extracellular matrix through their adhesion complexes, which were not investigated in this study. Further investigations are needed to understand the cellular events and potential changes in SMC mechanosensing in our model.

Our findings are broadly consistent with the idea that vascular remodeling occurs to maintain preferred homeostatic mechanical stress levels in the vascular wall (57). In this scenario, adventitial collagen would remodel in a more circumferential direction in older mice on the Western diet, in order to maintain stress homeostasis when active forces (basal tone) are reduced. The increase in adventitial collagen fiber angle with age in mice on the chow diet is more difficult to explain, but it may reflect increasing longitudinal tension in the aorta due to growth, as reflected in the significantly higher body weights of the older mice. The balance between these opposing effects—increased longitudinal tension and loss of basal tone—would then determine the final direction of collagen remodeling (44). These observations are consistent with recent work by Krasny et al. (58), which has shown that adventitial collagen fiber bundles transiently deform in

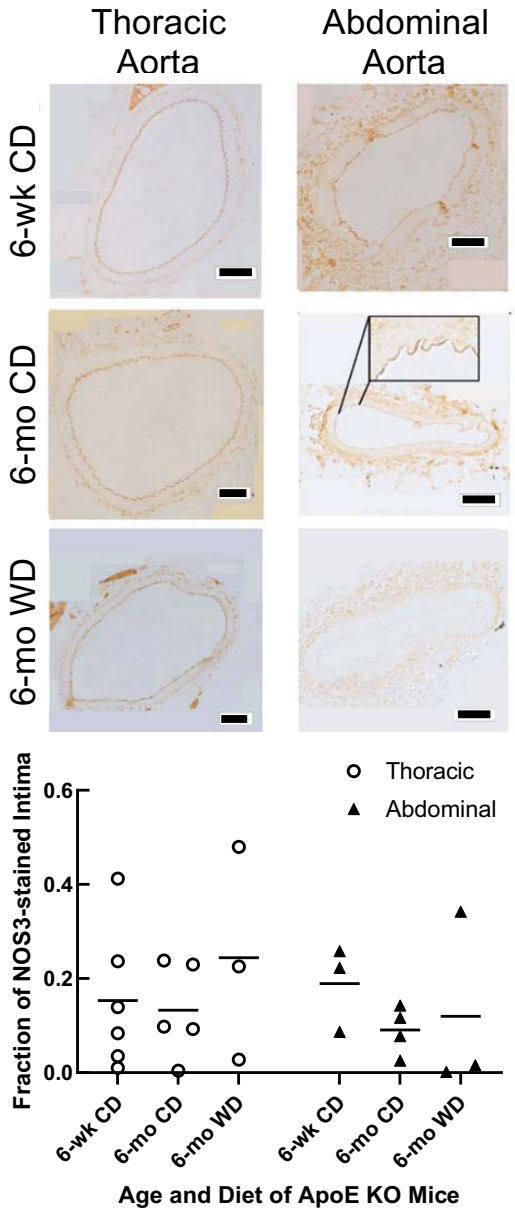

Figure 9. *Top left*: representative immunoperoxidase staining of arterial sections of apolipoprotein E knockout (apoE KO) mice taken from the thoracic aorta at the level of the 4th intercostal arteries for each of the three diet/age groups. *Top right*:: immunoperoxidase staining of aortic sections of apoE KO mice taken from the infrarenal abdominal aorta for each of the three diet/age groups. Scale bars = 10 μm. *Bottom*: quantitation of fractional nitric oxide synthase 3 (NOS3) staining of aortic intima as a function of age and diet (6 wk chow: $n = 3$ abdominal, $n = 6$ thoracic; 6 mo chow: $n = 4$ abdominal, $n = 5$ thoracic; 6 mo Western diet: $n = 3$ per location). No significant differences among groups were detected by ANOVA.

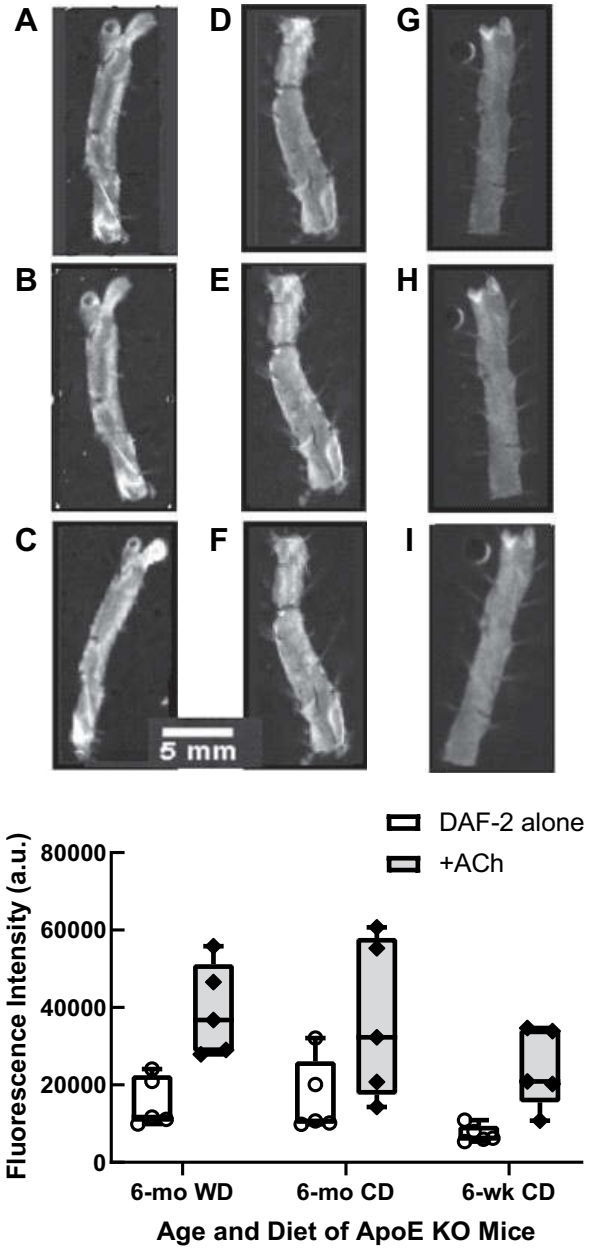

Figure 10. *Top*: representative examples of 4,5-diaminofluorescein (DAF-2) fluorescence indicative of basal and acetylcholine (ACh)-stimulated nitric oxide (NO) release in longitudinally-opened thoracic aortas of apolipoprotein E knockout (apoE KO) mice. *A*, *D*, *G*: baseline autofluorescence. *B*, *E*, *H*: DAF-2 only. *C*, *F*, *I*: DAF-2 plus acetylcholine. *A–C*: 6-mo Western diet. *D–F*: 6-mo chow diet. *G–I*: 6 wk chow diet. *Bottom*: quantitation of mean basal and ACh-induced NO release, as demonstrated by DAF-2 fluorescence ($n = 5$ mice per group). Two-way ANOVA showed that the addition of ACh significantly increased fluorescence intensity ($P < 0.001$), but there was no effect of treatment group.

a nonaffine fashion in response to changes in biaxial loading. Our in vivo studies suggest the possibility that such transient deformations might guide the direction of long-term vascular remodeling as well, leading to a long-lasting alteration in average collagen fiber orientation.

Previous simulations of the mechanical behavior of arteries have shown that there is an "optimum" value of collagen fiber angles, which enables the vessel to meet the mechanical condition $dF_z/dP = 0$ at the in vivo axial stretch ratio, where F_z is the axial force and P is the internal pressure (59). When this condition is met, axial forces on the vessel are minimized during the pressure swings of the cardiac cycle, likely reducing wear on surrounding connective tissue structures. For thin-walled arteries having only helically oriented fibers, the optimum fiber angle is given by the equation:

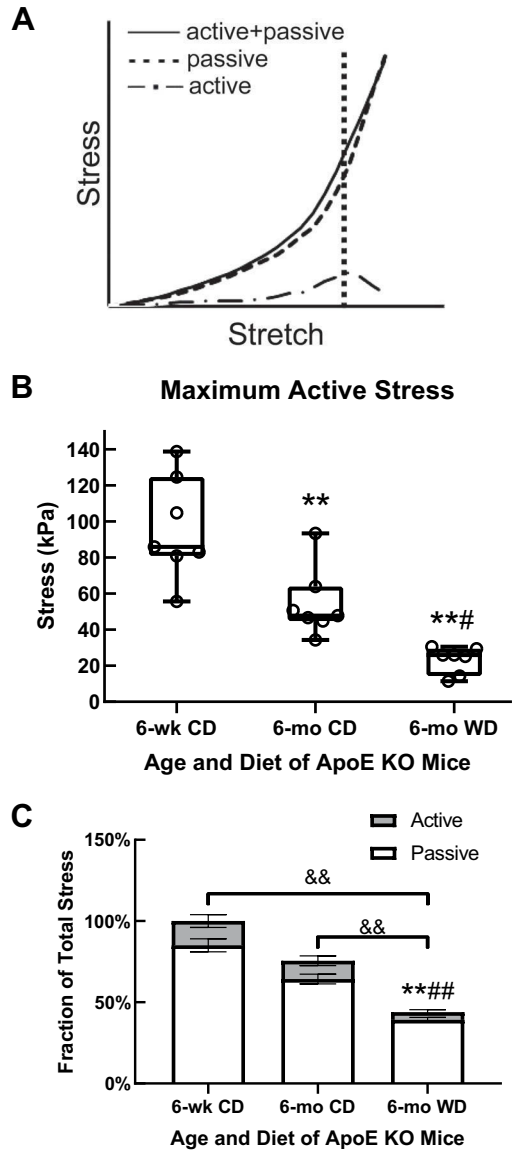

Figure 11. Maximum active stress generated by smooth muscle cells in the descending thoracic aorta of the apolipoprotein E knockout (apoE KO) mice at different ages and diets [chow (CD) and Western diet (WD)] obtained using wire myography ($n = 7$ for each diet group). *A*: schematic showing active stress as the difference between stress-strain curves for fully contracted (solid line, phenylephrine-treated) and fully relaxed (dashed line, SNP-treated) aortic rings. Dotted vertical line indicates stretch at maximum active stress. *B*: averaged results for maximum active stress. $^{**}P < 0.01$ vs. 6 wk, $\#P < 0.05$ vs. 6 mo CD by one-way ANOVA followed by Tukey multiple comparisons test. *C*: relative contribution of active stress to total stress measured at stretch value corresponding to peak active stress. % Active stress: $^{**}P < 0.01$ vs. 6 wk; $\#\#P < 0.01$ vs. 6 mo. CD. % Passive stress: $\&\&P < 0.01$ vs. 6 wk, $P < 0.01$ vs. 6 mo CD. Two-way ANOVA was performed followed by Tukey multiple-comparisons test.

$$F_z \approx \pi r_i^2 P(2tan^2(\beta) - 1)$$

where r_i is the internal radius and β is the fiber angle, yielding a value of β = 35.3° (59).

Fibers oriented in a more longitudinal direction relative to the optimum angle would be associated with increased axial tension as blood pressure increases during systole, and fibers oriented in a more circumferential direction relative to the optimum would be associated with reduced axial tension (recoil, or possibly even compression) during systole.

Conclusions

We show here that collagen fiber angular distribution diverges with aging in apoE KO mice on chow diet versus those on Western diet. Our data indicate that the aortas of 6-wk-old apoE KO mice have a significantly lower mean collagen fiber angle when compared to older mice (6 mo) on chow diet, but a significantly greater mean fiber angle compared to 7.5-mo-old mice on a Western diet. These differences show that proatherogenic diet alters age-related collagen remodeling.

In addition, we demonstrate using in vivo physiological measurements that alterations in adventitial collagen fiber angle distribution cannot be attributed to significant changes in aortic hemodynamics. We did not detect significant changes in volumetric blood flow rates or macro-level structural changes (aortic diameter) in either the thoracic or abdominal regions that were sampled for collagen fiber angle measurements. Furthermore, we have sampled in areas without lesions, ruling out pathological wall remodeling specific to plaque development.

We have demonstrated that, starting with an average fiber angle of 36° in young adult mice, collagen fiber reorientation with aging can result either in more longitudinally oriented fibers or in more circumferentially oriented fibers, depending on diet. Although Western diet feeding is known to have many biochemical and physiological consequences in apoE KO mice (60), we have focused here on its role in altering the balance between passive and active stresses in the vessel wall, either by promoting endothelial dysfunction or by altering basal smooth muscle tone. We directly measured acetylcholine-mediated nitric oxide release via diaminofluorescein-2 diacetate (DAF-2 DA) and active force generation in the arterial wall via wire myography. We found no significant decrease in NO release with age; thus, endothelial dysfunction is unlikely to be the cause of collagen remodeling in our model. In contrast, we found a significant decrease in active stress generation, as well as in the relative contribution of active stress to total wall stress in mice at 6 mo of age compared to 6-wk-old mice, which was further exacerbated by Western diet feeding. These results suggest that loss of SMC basal tone, which is further enhanced by proatherogenic stimuli, may act as a mechanical stimulus for collagen fiber reorganization during aging.

One limitation of the current study is the use of wire myography rather than biaxial mechanical testing to assess vascular contractility (61), which did not allow us to determine whether longitudinal tension also changes with aging in mice on a chow diet or Western diet. It should also be noted that volumetric flow measurements by ultrasound are subject to several sources of error, including failure to position the probe head accurately to acquire centerline velocities, variations in depth of anesthesia that can alter cardiac output, and variations in angle of probe relative to mean flow direction. In addition, further studies that include B6 wild-type mice will be needed to fully parse out the relative contributions of age, diet, and susceptibility to atherosclerosis to collagen fiber remodeling. Potentially productive avenues for future work would include investigating mechanisms responsible for reducing active mechanical response in atherosclerotic vessels. In addition, the complex interactions among hemodynamics, vascular contractility, and matrix remodeling motivate continued development of mathematical models capable of simulating vascular remodeling and of delineating the relative importance of multiple contributing factors.

ACKNOWLEDGMENTS

We gratefully acknowledge John A. Johnson and Marcella Marks for their assistance with experimental studies.

GRANTS

This work received funding from National Science Foundation through Grants CMMI-1200358 and CMMI-1760906 and National Institutes of Health Grants EB019663-01A1, HL145064-01, and HL133662-01A1. Continuity software was developed and provided by the National Biomedical Computation Resource under National Center for Research Resources Grant 5P41RR008605-19 and National Institute of General Medical Sciences Grant 8 P41 GM103426-19.

DISCLAIMERS

The funding organizations played no role in the study design, data analysis, manuscript preparation, or decision to publish.

DISCLOSURES

No conflicts of interest, financial or otherwise, are declared by the authors.

AUTHOR CONTRIBUTIONS

S.M.L. and E.A.P. conceived and designed research; S.R.W., K. M.C., N.G., L.D., and S.M.H. performed experiments; S.R.W., S.M.L., K.M.C., P.L., N.G., L.D., S.M.H., and J.F.E. analyzed data; S.R.W., S. M.L., P.L., N.G., L.D., E.A.P., M.A.S., and J.F.E. interpreted results of experiments; S.R.W., K.M.C., P.L., N.G. and L.D. prepared figures; S.R.W., K.M.C. and N.G. drafted manuscript; S.R.W., S.M.L., P.L., E. A.P., M.A.S., and J.F.E. edited and revised manuscript; S.R.W. and S.M.L. approved final version of manuscript.

REFERENCES

1. **Gaballa MA**, **Jacob CT**, **Raya TE**, **Liu J**, **Simon B**, **Goldman**, **S.** Large artery remodeling during aging: biaxial passive and active stiffness. *Hypertension* 32: 437–443, 1998. doi:10.1161/01.HYP.32.3.437.
2. **Greenwald SE.** Ageing of the conduit arteries. *J Pathol* 211: 157–172, 2007. doi:10.1002/path.2101.
3. **Hayashi K**, **Naiki**, **T.** Adaptation and remodeling of vascular wall; biomechanical response to hypertension. *J Mech Behav Biomed Mater* 2: 3–19, 2009. doi:10.1016/j.jmbbm.2008.05.002.
4. **Lemarié CA**, **Tharaux P-L**, **Lehoux**, **S.** Extracellular matrix alterations in hypertensive vascular remodeling. *J Mol Cell Cardiol* 48: 433–439, 2010. doi:10.1016/j.yjmcc.2009.09.018.

5. **Wu J**, **Montaniel KRC**, **Saleh MA**, **Xiao L**, **Chen W**, **Owens GK**, **Humphrey JD**, **Majesky MW**, **Paik DT**, **Hatzopoulos AK**, **Madhur MS**, **Harrison**, **DG.** Origin of matrix-producing cells that contribute to aortic fibrosis in hypertension. *Hypertension* 67: 461–468, 2016. doi:10.1161/HYPERTENSIONAHA.115.06123.
6. **Wang JC**, **Bennett**, **M.** Aging and atherosclerosis: mechanisms, functional consequences, and potential therapeutics for cellular senescence. *Circ Res* 111: 245–259, 2012. doi:10.1161/CIRCRESAHA.111.261388.
7. **Plump AS**, **Smith JD**, **Hayek T**, **Aalto-Setälä K**, **Walsh A**, **Verstuyft JG**, **Rubin EM**, **Breslow**, **JL.** Severe hypercholesterolemia and atherosclerosis in apolipoprotein E-deficient mice created by homologous recombination in ES cells. *Cell* 71: 343–353, 1992. doi:10.1016/0092-8674(92)90362-G.
8. **Zhang SH**, **Reddick RL**, **Piedrahita JA**, **Maeda**, **N.** Spontaneous hypercholesterolemia and arterial lesions in mice lacking apolipoprotein E. *Science* 258: 468–471, 1992. doi:10.1126/science.1411543.
9. **Nakashima Y**, **Plump AS**, **Raines EW**, **Breslow JL**, **Ross**, **R.** ApoE-deficient mice develop lesions of all phases of atherosclerosis throughout the arterial tree. *Arterioscler Thromb* 14: 133–140, 1994. doi:10.1161/01.ATV.14.1.133.
10. **Fetterman JL**, **Pompilius M**, **Westbrook DG**, **Uyeminami D**, **Brown J**, **Pinkerton KE**, **Ballinger**, **SW.** Developmental exposure to secondhand smoke increases adult atherogenesis and alters mitochondrial DNA copy number and deletions in apoE−/− mice. *PloS One* 8: e66835, 2013. doi:10.1371/journal.pone.0066835.
11. **Weingärtner O**, **Husche C**, **Schött HF**, **Speer T**, **Böhm M**, **Miller CM**, **McCarthy F**, **Plat J**, **Lütjohann D**, **Laufs**, **U.** Vascular effects of oxysterols and oxyphytosterols in apoE−/− mice. *Atherosclerosis* 240: 73–79, 2015. doi:10.1016/j.atherosclerosis.2015.02.032.
12. **Yi X**, **Xu L**, **Kim K**, **Kim H-S**, **Maeda** , **N.** Genetic reduction of lipoic acid synthase expression modestly increases atherosclerosis in male, but not in female, apolipoprotein E-deficient mice. *Atherosclerosis* 211: 424–430, 2010. doi:10.1016/j.atherosclerosis.2010.03.009.
13. **Burleigh MC**, **Briggs AD**, **Lendon CL**, **Davies MJ**, **Born GV**, **Richardson**, **PD.** Collagen types I and III, collagen content, GAGs and mechanical strength of human atherosclerotic plaque caps: span-wise variations. *Atherosclerosis* 96: 71–81, 1992. doi:10.1016/0021-9150(92)90039-j.
14. **Finn AV**, **Nakano M**, **Narula J**, **Kolodgie FD**, **Virmani**, **R.** Concept of vulnerable/unstable plaque. *Arterioscler Thromb Vasc Biol* 30: 1282–1292, 2010. doi:10.1161/ATVBAHA.108.179739.
15. **Luttun A**, **Lupu F**, **Storkebaum E**, **Hoylaerts MF**, **Moons L**, **Crawley J**, **Bono F**, **Poole AR**, **Tipping P**, **Herbert J-M**, **Collen D**, **Carmeliet**, **P.** Lack of plasminogen activator inhibitor-1 promotes growth and abnormal matrix remodeling of advanced atherosclerotic plaques in apolipoprotein E-deficient mice. *Arterioscler Thromb Vasc Biol* 22: 499–505, 2002. doi:10.1161/hq0302.104529.
16. **Rosenfeld ME**, **Polinsky P**, **Virmani R**, **Kauser K**, **Rubanyi G**, **Schwartz**, **SM.** Advanced atherosclerotic lesions in the innominate artery of the ApoE knockout mouse. *Arterioscler Thromb Vasc Biol* 20: 2587–2592, 2000. doi:10.1161/01.ATV.20.12.2587.
17. **Wang Y**, **Johnson JA**, **Fulp A**, **Sutton MA**, **Lessner**, **SM.** Adhesive strength of atherosclerotic plaque in a mouse model depends on local collagen content and elastin fragmentation. *J Biomech* 46: 716–722, 2013. doi:10.1016/j.jbiomech.2012.11.041.
18. **Bentzon JF**, **Pasterkamp G**, **Falk**, **E.** Expansive remodeling is a response of the plaque-related vessel wall in aortic roots of ApoE-deficient mice. *Arteriosclerosis, Thrombosis, and Vascular Biology* 23: 257–262, 2003. doi:10.1161/01.ATV.0000051387.70962.79.
19. **Glagov S**, **Weisenberg E**, **Zarins CK**, **Stankunavicius R**, **Kolettis** , **GJ.** Compensatory enlargement of human atherosclerotic coronary arteries. *N Engl J Med* 316: 1371–1375, 1987. doi:10.1056/NEJM198705283162204.
20. **Topol EJ**, **Nissen**, **SE.** Our preoccupation with coronary luminology. *Circulation* 92: 2333–2342, 1995. doi:10.1161/01.CIR.92.8.2333.
21. **Akyildiz AC**, **Chai C-K**, **Oomens CWJ**, **van der Lugt A**, **Baaijens FPT**, **Strijkers GJ**, **Gijsen**, **FJH.** 3D fiber orientation in atherosclerotic carotid plaques. *J Struct Biol* 200: 28–35, 2017. doi:10.1016/j.jsb.2017.08.003.
22. **Agianniotis A**, **Stergiopulos**, **N.** Wall properties of the apolipoprotein E-deficient mouse aorta. *Atherosclerosis* 223: 314–320, 2012. doi:10.1016/j.atherosclerosis.2012.06.014.
23. **Cilla M**, **Pérez M**, **Peña E**, **Martínez**, **M.** Effect of diet and age on arterial stiffening due to atherosclerosis in ApoE−/− mice. *Ann Biomed Eng* 44: 2202–2217, 2016. doi:10.1007/s10439-015-1486-1.
24. **Hadi HA**, **Carr CS**, **Al Suwaidi**, **J.** Endothelial dysfunction: cardiovascular risk factors, therapy, and outcome. *Vasc Health Risk Manag* 1: 183–198, 2005.
25. **Park K-H**, **Park**, **WJ.** Endothelial dysfunction: clinical implications in cardiovascular disease and therapeutic approaches. *J Korean Med Sci* 30: 1213–1225, 2015. doi:10.3346/jkms.2015.30.9.1213.
26. **Rudic RD**, **Shesely EG**, **Maeda N**, **Smithies O**, **Segal SS**, **Sessa**, **WC.** Direct evidence for the importance of endothelium-derived nitric oxide in vascular remodeling. *J Clin Invest* 101: 731–736, 1998. doi:10.1172/JCI1699.
27. **Valentín A**, **Cardamone L**, **Baek S**, **Humphrey**, **J.** Complementary vasoactivity and matrix remodelling in arterial adaptations to altered flow and pressure. *J R Soc Interface* 6: 293–306, 2009. doi:10.1098/rsif.2008.0254.
28. **Watson SR**, **Liu P**, **Peña EA**, **Sutton MA**, **Eberth JF**, **Lessner**, **SM.** Comparison of aortic collagen fiber angle distribution in mouse models of atherosclerosis using second-harmonic generation (SHG) microscopy. *Microsc Microanal* 22: 55–62, 2016. doi:10.1017/S1431927615015585.
29. **Liu H**, **Qin W**, **Ma Z**, **Gao BZ**, **Shao Y**, **Ye T**, **Borg**, **TK.** Myofibrillogenesis in live neonatal cardiomyocytes observed with hybrid two-photon excitation fluorescence-second harmonic generation microscopy. *J Biomed Opt* 16: 126012, 2011. doi:10.1117/1.3662457.
30. **Liu H**, **Shao Y**, **Qin W**, **Runyan RB**, **Xu M**, **Ma Z**, **Borg TK**, **Markwald R**, **Gao**, **BZ.** Myosin filament assembly onto myofibrils in live neonatal cardiomyocytes observed by TPEF-SHG microscopy. *Cardiovasc Res* 97: 262–270, 2013. doi:10.1093/cvr/cvs328.
31. **Wicker BK**, **Hutchens HP**, **Wu Q**, **Yeh AT**, **Humphrey**, **JD.** Normal basilar artery structure and biaxial mechanical behaviour. *Comput Methods Biomech Biomed Engin* 11: 539–551, 2008. doi:10.1080/10255840801949793.
32. **Ozaki M**, **Kawashima S**, **Yamashita T**, **Hirase T**, **Namiki M**, **Inoue N**, **Hirata K-I**, **Yasui H**, **Sakurai H**, **Yoshida Y**, **Masada M**, **Yokoyama**, **M.** Overexpression of endothelial nitric oxide synthase accelerates atherosclerotic lesion formation in apoE-deficient mice. *J Clin Invest* 110: 331–340, 2002. doi:10.1172/JCI0215215.
33. **Finlay HM**, **McCullough L**, **Canham**, **PB.** Three-dimensional collagen organization of human brain arteries at different transmural pressures. *J Vasc Res* 32: 301–312, 1995. doi:10.1159/000159104.
34. **Collins M**, **Bersi M**, **Wilson E**, **Humphrey**, **J.** Mechanical properties of suprarenal and infrarenal abdominal aorta: implications for mouse models of aneurysms. *Med Eng Phys* 33: 1262–1269, 2011. doi:10.1016/j.medengphy.2011.06.003.
35. **Ferruzzi J**, **Madziva D**, **Caulk A**, **Tellides G**, **Humphrey**, **J.** Compromised mechanical homeostasis in arterial aging and associated cardiovascular consequences. *Biomech Model Mechanobiol* 17: 1281–1295, 2018. doi:10.1007/s10237-018-1026-7.
36. **Gibbons GH**, **Dzau**, **VJ.** The emerging concept of vascular remodeling. *N Engl J Med* 330: 1431–1438, 1994. doi:10.1056/NEJM199405193302008.
37. **Zarins CK**, **Zatina MA**, **Giddens DP**, **Ku DN**, **Glagov**, **S.** Shear stress regulation of artery lumen diameter in experimental atherogenesis. *J Vasc Surg* 5: 413–420, 1987. doi:10.1067/mva.1987.avs0050413.
38. **Arruda RM**, **Peotta VA**, **Meyrelles SS**, **Vasquez**, **EC.** Evaluation of vascular function in apolipoprotein E knockout mice with angiotensin-dependent renovascular hypertension. *Hypertension* 46: 932–936, 2005. doi:10.1161/01.HYP.0000182154.61862.52.
39. **Barton M**, **Haudenschild CC**, **d'Uscio LV**, **Shaw S**, **Münter K**, **Lüscher**, **TF.** Endothelin ETA receptor blockade restores NO-mediated endothelial function and inhibits atherosclerosis in apolipoprotein E-deficient mice. *Proc Natl Acad Sci* 95: 14367–14372, 1998. doi:10.1073/pnas.95.24.14367.
40. **d'Uscio LV**, **Barton M**, **Shaw S**, **Lüscher**, **TF.** Chronic ETA receptor blockade prevents endothelial dysfunction of small arteries in apolipoprotein E-deficient mice. *Cardiovasc Res* 53: 487–495, 2002. doi:10.1016/s0008-6363(01)00469-2.
41. **Gervais M**, **Pons S**, **Nicoletti A**, **Cosson C**, **Giudicelli J-F**, **Richer**, **C.** Fluvastatin prevents renal dysfunction and vascular NO deficit in apolipoprotein E-deficient mice. *Arterioscler Thromb Vasc Biol* 23: 183–189, 2003. doi:10.1161/01.ATV.0000051404.84665.49.

42. **Nogueira BV**, **Peotta VA**, **Meyrelles SS**, **Vasquez**, **EC.** Evaluation of aortic remodeling in apolipoprotein E-deficient mice and renovascular hypertensive mice. *Arch Med Res* 38: 816–821, 2007. doi:10.1016/j.arcmed.2007.06.005.
43. **Yang R**, **Powell-Braxton L**, **Ogaoawara AK**, **Dybdal N**, **Bunting S**, **Ohneda O**, **Jin**, **H.** Hypertension and endothelial dysfunction in apolipoprotein E knockout mice. *Arterioscler Thromb Vasc Biol* 19: 2762–2768, 1999. doi:10.1161/01.ATV.19.11.2762.
44. **Driessen NJB**, **Cox MAJ**, **Bouten CVC**, **Baaijens**, **FPT.** Remodelling of the angular collagen fiber distribution in cardiovascular tissues. *Biomech Model Mechanobiol* 7: 93, 2008. doi:10.1007/s10237-007-0078-x.
45. **Eberth J**, **Cardamone L**, **Humphrey**, **J.** Evolving biaxial mechanical properties of mouse carotid arteries in hypertension. *J Biomech* 44: 2532–2537, 2011. doi:10.1016/j.jbiomech.2011.07.018.
46. **Amirbekian S**, **Long RC, Jr**, **Consolini MA**, **Suo J**, **Willett NJ**, **Fielden SW**, **Giddens DP**, **Taylor WR**, **Oshinski**, **JN.** In vivo assessment of blood flow patterns in abdominal aorta of mice with MRI: implications for AAA localization. *Am J Physiol-Heart Circ Physiol* 297: H1290–H1295, 2009. doi:10.1152/ajpheart.00889.2008.
47. **Bonthu S**, **Heistad DD**, **Chappell DA**, **Lamping KG**, **Faraci**, **FM.** Atherosclerosis, vascular remodeling, and impairment of endothelium-dependent relaxation in genetically altered hyperlipidemic mice. *Arterioscler Thromb, Vasc Biol* 17: 2333–2340, 1997. doi:10.1161/01.ATV.17.11.2333.
48. **Johansson ME**, **Ulrika H**, **Wikström J**, **Wickman A**, **Bergström G**, **Gan**, **L.** Haemodynamically significant plaque formation and regional endothelial dysfunction in cholesterol-fed ApoE−/− mice. *Clin Sci* 108: 531–538, 2005. doi:10.1042/CS20040322.
49. **Deckert V**, **Lizard G**, **Duverger N**, **Athias A**, **Palleau V**, **Emmanuel F**, **Moisant M**, **Gambert P**, **Lallemant C**, **Lagrost**, **L.** Impairment of endothelium-dependent arterial relaxation by high-fat feeding in ApoE-deficient mice: toward normalization by human ApoA-I expression. *Circulation* 100: 1230–1235, 1999. doi:10.1161/01.cir.100.11.1230.
50. **Jiang F**, **Gibson AP**, **Dusting**, **GJ.** Endothelial dysfunction induced by oxidized low-density lipoproteins in isolated mouse aorta: a comparison with apolipoprotein-E deficient mice. *Eur J Pharmacol* 424: 141–149, 2001. doi:10.1016/s0014-2999(01)01140-2.
51. **Crauwels HM**, **Van Hove CE**, **Holvoet P**, **Herman AG**, **Bult**, **H.** Plaque-associated endothelial dysfunction in apolipoprotein E-deficient mice on a regular diet. Effect of human apolipoprotein AI. *Cardiovasc Res* 59: 189–199, 2003. doi:10.1016/S0008-6363(03)00353-5.
52. **Guns P**, **Van Assche T**, **Verreth W**, **Fransen P**, **Mackness B**, **Mackness M**, **Holvoet P**, **Bult**, **H.** Paraoxonase 1 gene transfer lowers vascular oxidative stress and improves vasomotor function in apolipoprotein E-deficient mice with pre-existing atherosclerosis. *Br J Pharmacol* 153: 508–516, 2008. doi:10.1038/sj.bjp.0707585.
53. **Owens GK**, **Kumar MS**, **Wamhoff**, **BR.** Molecular regulation of vascular smooth muscle cell differentiation in development and disease. *Physiol Rev* 84: 767–801, 2004. doi:10.1152/physrev.00041.2003.
54. **Gomez D**, **Owens**, **GK.** Smooth muscle cell phenotypic switching in atherosclerosis. *Cardiovasc Res* 95: 156–164, 2012. doi:10.1093/cvr/cvs115.
55. **Mayr M**, **Xu**, **Q.** Smooth muscle cell apoptosis in arteriosclerosis. *Exp Gerontol* 36: 969–987, 2001. doi:10.1016/S0531-5565(01)00090-0.
56. **Humphrey JD**, **Milewicz DM**, **Tellides G**, **Schwartz**, **MA.** Cell biology. Dysfunctional mechanosensing in aneurysms. *Science* 344: 477–479, 2014. doi:10.1126/science.1253026.
57. **Humphrey JD.** Vascular mechanics, mechanobiology, and remodeling. *J Mech Med Biol* 09: 243–257, 2009. doi:10.1142/S021951940900295X.
58. **Krasny W**, **Morin C**, **Magoariec H**, **Avril**, **S.** A comprehensive study of layer-specific morphological changes in the microstructure of carotid arteries under uniaxial load. *Acta Biomater* 57: 342–351, 2017. doi:10.1016/j.actbio.2017.04.033.
59. **Avril S**, **Badel P**, **Gabr M**, **Sutton MA**, **Lessner**, **SM.** Biomechanics of porcine renal arteries and role of axial stretch. *J Biomech Eng* 135: 81007–81010, 2013. doi:10.1115/1.4024685.
60. **Vasquez EC**, **Peotta VA**, **Gava AL**, **Pereira TM**, **Meyrelles**, **SS.** Cardiac and vascular phenotypes in the apolipoprotein E-deficient mouse. *J Biomed Sci* 19: 22, 2012. doi:10.1186/1423-0127-19-22.
61. **Zhou B**, **Prim DA**, **Romito EJ**, **McNamara LP**, **Spinale FG**, **Shazly T**, **Eberth**, **JF.** Contractile smooth muscle and active stress generation in porcine common carotids. *J Biomech Eng* 140: 014501–0145016, 2018. doi:10.1115/1.4037949.